Advantage of GaN in Phase Shift Full Bridges

Feng Qi, Zhan Wang, Yifeng Wu, and Philip Zuk

Transphorm Inc.
Goleta, CA 93117

Abstract—**GaN FET and Si MOSFET have very different voltage dependence of output capacitance (C_{oss}). Due to the difference, GaN FET offers low C_{oss} stored charge (Q_{oss}) while Si MOSFET gives low C_{oss} stored energy (E_{oss}). As low Q_{oss} benefits reduction of resonant energy and time, GaN FET is ideal for resonant type of half or full bridges requiring low resonant energy and short resonant time. And, low E_{oss} makes Si MOSFET a great candidate for single switch hard switching applications. In this paper, detailed comparative analysis between GaN FET and Si MOSFETs is conducted for resonance in Phase Shift Full Bridge converters (PSFB). Following the analysis, a 200 kHz 3.3 kW PSFB for on-board charger application is built and evaluated in order to demonstrate the advantages of GaN FETs.**

Keywords—GaN, Phase Shift Full Bridge, Soft Switching

I. INTRODUCTION

PSFB is a classic soft switching topology. It offers high voltage conversion ratio, low output current ripple, and simple phase shift control. In decades, it has been widely applied in power supply and battery chargers. Si device was the only choice for PSFB before emerging of wide band gap devices. As PSFB easily loses zero voltage switching (ZVS) at light load due to lacking resonant energy, novel devices with lower Q_{oss}, like GaN FET, can significantly expand its ZVS region and reduce the required resonant energy.

As a forerunner of wide band gap devices, Transphorm's 650V GaN FETs have been built into active front end of premium power supplies, such as Bel Power TET3000-12-069RA and CORSAIR AX1600i [1-2]. The recent ramp-up of adoption in the market is a result of not only performance but also maturity of the Cascode GaN FETs [3-5]. The GaN FETs offer advantages not only in hard switching converters, like totem pole PFC, but also in converters with conditional hard switching region, such as Dual Active Bridge (DAB) and PSFB. In DAB, performance of DAB based on Si, SiC and GaN has been well discussed in [6 - 8]. Other than devices, soft switching region of DAB can also be greatly extended by advanced modulation technology [9]. In PSFB, due to its limits in modulation method, soft switching region is primarily determined by Q_{oss} and resonant inductance. It is critical to take advantage of devices characteristics. A great example of SiC based PSFB is given in [10]. This paper focuses on comparative analysis of GaN and Si in ZVS and partial ZVS region of PSFB.

PSFB achieves soft switching via resonance between Q_{oss} and resonant inductance. Fully completed resonance offers ZVS. Partially completed resonance results in partial ZVS or even non-ZVS. The transition from ZVS to non-ZVS is a complex process. It highly depends on the characteristics of Q_{oss}. By analyzing the transition, the characteristics of GaN and Si are compared in full and partial resonance, and the advantage of GaN is highlighted in the discussion.

The following sections include analysis of GaN's advantage in PSFB and evaluation of a prototype built with 650V 72mΩ GaN FETs. The prototype is a 200 kHz 3.3kW PSFB converter designed for 400V battery charger and designed for demonstration of the GaN FETs.

II. COMPARATIVE ANALYSIS

GaN TPH3212PS and Si IPP60R090CFD7, are studied in the comparative analysis. The Q_{oss} and E_{oss} curves of the devices are drawn in Fig. 1 as a function of V_{ds}. Voltage dependence of Q_{oss} and E_{oss} are very different for GaN and Si. Q_{oss} and E_{oss} of GaN FET are gradually accumulated over the whole voltage range while those of Si MOSFET are mostly accumulated at low voltage region. This results in very different resonant behavior.
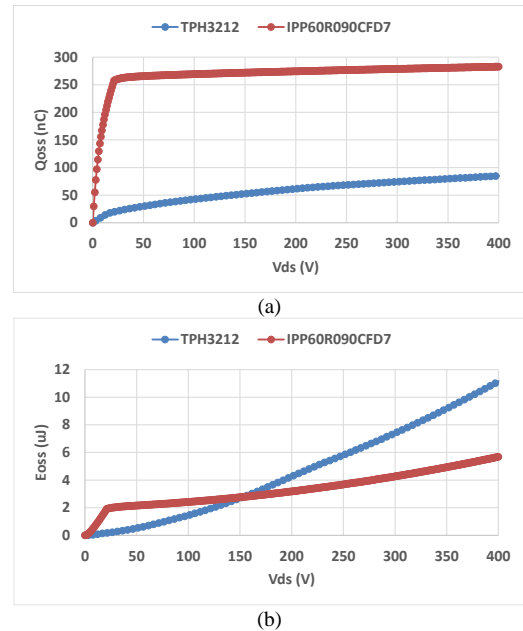

(a)

(b)

Fig. 1 (a) Q_{oss} .vs Vds curve, and (b) E_{oss} .vs Vds curve from 0V to 400V

The goal of the analysis is to find the best device for a 200 kHz 3.3 kW PSFB targeting at on-board charger with input from 380V to 410V and output from 250V to 450V as shown in Fig. 2. Parameters are summarized in Table I. The DC blocking capacitor can be removed in peak current mode control. An active snubber in Fig. 3 is implemented at secondary side to improve efficiency of snubber [11]. Its parameters are summarized in Table II.
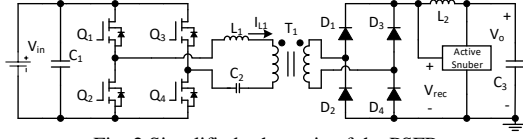

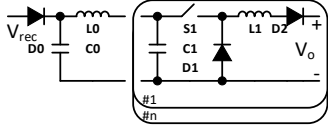Fig. 2 Simplified schematic of the PSFB

Fig. 3 Simplified schematic of the active snubber

Table I Parameters of the PSFB

DC-link Voltage (V)	380 ~ 410
Battery Voltage (V)	250 ~ 450
Maximum Power (W)	3300
Maximum Current (A)	11
Switching frequency (kHz)	200
Transformer turns ratio	1:1.18
Leakage inductance (μH)	1.0
Resonant inductor (μH)	1.7
Output inductor (μH)	65
DC blocking capacitor (μF)	5

Table II Parameters of the active snubber

C0 (μF)	0.5
L0 (μH)	10
C1 (μF)	0.2
L1 (μH)	2700
D0	SCS206
S1	NCP1060AD100
D1, D2	ES1J

In the following discussion, the switching transition after Q1 turned-off is studied for both soft and hard switching. In PSFB, boundary condition between full ZVS and partial ZVS is sketched in Fig. 4 (a). At the boundary condition, energy stored in L1 is just enough to complete ZVS, and the dead time, t_{db}, is just equal to the resonant time, t_{res}. For the ideal case in Fig. 4 (a), circuit analysis during the resonance is illustrated in equivalent circuits Fig. 4 (b) to (e), I_{L1_1} is the current of L1 at the start of resonance, and I_{L1_2} is the current at the end of resonance. In Fig. 4, Q1 is turned off at t1, and Q2 is turned on at t2. A zero voltage soft switching transition is accomplished during the dead time t_{db}. During this process, C_{oss} of Q1 is charged from 0V to V_{dc}, and C_{oss} of Q2 is discharged from V_{dc} to 0V. In other words, $Q_{oss(0V)To(Vdc)}$ and $E_{oss(0V)To(Vdc)}$ are injected to Q1, and $Q_{oss(Vdc)To(0V)}$ and $E_{oss(Vdc)To(0V)}$ are removed from Q2. Meanwhile, $Q_{oss(Vdc)To(0V)} \times V_{dc}$ are energized to the DC-link since the

discharging current of Q2 flows through the DC-link. The process is powered by the inductor current, I_{L1}. With the PSFB parameters in Table I, I_{L1_1} and I_{L1_2}, are calculated with Equ. (1) and (2), and summarized in Table III. From the results, GaN FET cuts both resonant time and current by over 40%. The reduction essentially expands the range of ZVS allowing dead time less than 100ns.
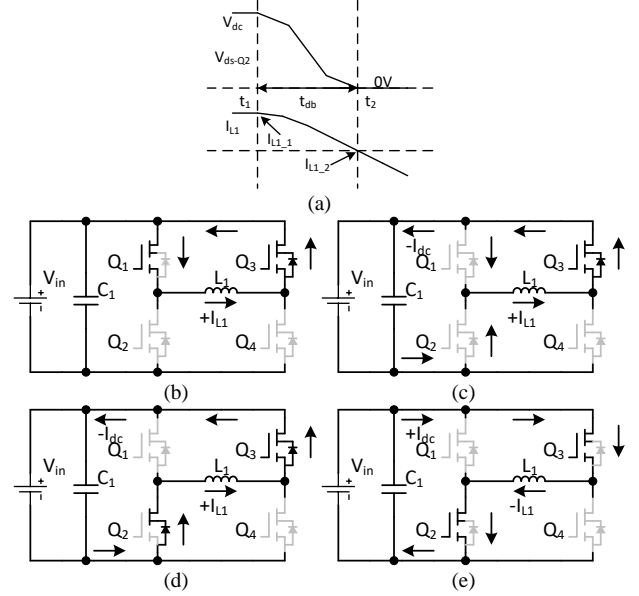

Fig. 4 Ideal soft switching waveform and simplified circuit diagram showing current flow (a) waveform, and current flow (b) before t1, (c) after t1, (d) before t2, (e) after t2

$$E_{oss(0V)To(Vdc)} + \left(Q_{oss(Vdc)To(0V)} \times V_{dc} - E_{oss(Vdc)To(0V)} \right)$$
$$= 0.5 \times L_1 \times \left(I_{L1\_1}^2 - I_{L1\_2}^2 \right) \qquad (1)$$
$$Q_{oss(0V)To(Vdc)} + Q_{oss(Vdc)To(0V)}$$
$$= 0.5 \times t_{db} \times \left(I_{L1\_1} + I_{L1\_2} \right) \qquad (2)$$

Table III ZVS boundary condition

	TPH3212PS	IPP60R090CFD7
$R_{on(tpy)}$ (mΩ)	72	75
$C_{o(tr)\_400V}$ (pF)	225	751
$C_{o(er)\_400V}$ (pF)	142	73
t_{res} (ns)	70	128
I_{L1_1} (A)	5.2	9.4
I_{L1_2} (A)	0	0

If the energy is less than that in the boundary condition, V_{ds} only drops to V_x as sketched in Fig. 5 (a) and Fig. 6 (a). V_x is the voltage of switching node at the end of resonance. The parameters, I_{L1_1}, I_{L1_2}, and V_x, are calculated with Equ. (3) and (4). During the resonance, $Q_{oss(0V)To(Vdc-Vx)}$ charges the device, which is being turned off, from 0V to $V_{dc} - V_x$, and $Q_{oss(Vdc)To(Vx)}$ discharges the device, which is going to be turned on, from V_{dc} to V_x. The subscripts carry the same meaning for the corresponding E_{oss} in the equations. As can be noted in Fig. 1, Q_{oss} and E_{oss} are function of V_x, which makes these cases more complex to solve. Due to non-linearity of the correlation between Q_{oss}, E_{oss} and V_x, the actual curves instead of approximated functions are used in the

calculation of V_x and charge related loss in a phase leg caused by partial ZVS at V_x in the following comparison.

$$E_{oss(0V)To(Vdc-Vx)} + \left(Q_{oss(Vdc)To(Vx)} \times V_{dc} - E_{oss(Vdc)To(Vx)}\right)$$
$$= 0.5 \times L_1 \times \left(I_{L1\_1}^2 - I_{L1\_2}^2\right) \quad (3)$$
$$Q_{oss(0V)To(Vdc-Vx)} + Q_{oss(Vdc)To(Vx)}$$
$$= 0.5 \times t_{db} \times \left(I_{L1\_1} + I_{L1\_2}\right) \quad (4)$$
$$\left(Q_{oss(Vdc-Vx)ToVdc} \times V_{dc} - E_{oss(Vdc-Vx)ToVdc}\right) + E_{oss(Vx)To(0V)}$$
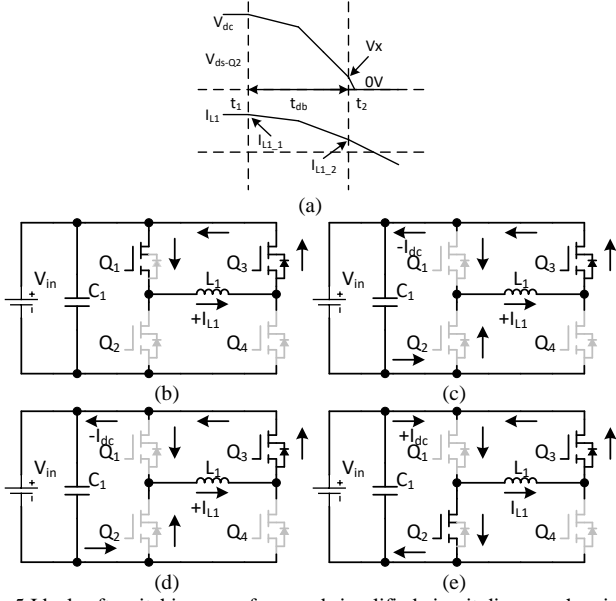$$= Loss\ of\ A\ Phase\ Leg \quad (5)$$

Fig. 5 Ideal soft switching waveform and simplified circuit diagram showing current flow (a) waveform, and current flow (b) before t1, (c) after t1, (d) before t2, (e) after t2
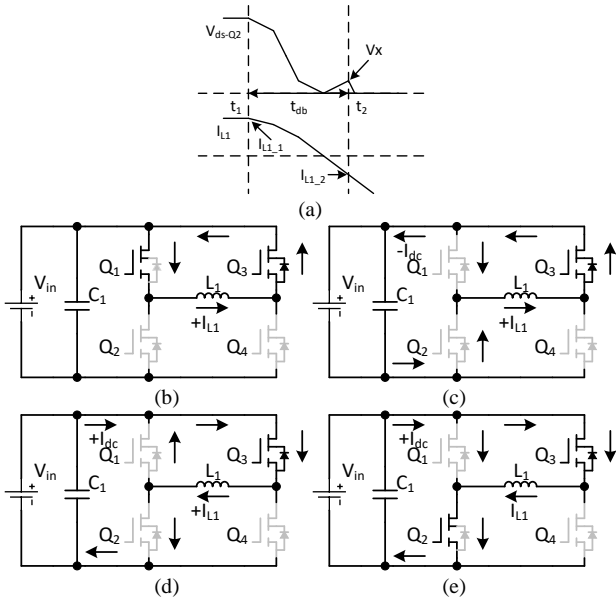

Fig. 6 Ideal soft switching waveform and simplified circuit diagram showing current flow (a) waveform, and current flow (b) before t1, (c) after t1, (d) before t2, (e) after t2

The V_x and the charge related loss are plotted as a function of I_{L1_1} in Fig. 5. GaN FET offers superior performance in ZVS and partial ZVS operation. GaN starts partial ZVS at I_{L1_1} much lower than that of Si, which significantly extended ZVS region. Furthermore, although both GaN and Si could be operated at the worst case, in which V_x equals to V_{dc}, 400V, GaN offers over 75% lower switching loss related to the remaining charge cause by V_x. In other words, Si MOSFET could suffer from junction to case temperature 4 times of that of GaN FETs and easily fall into thermal run away.
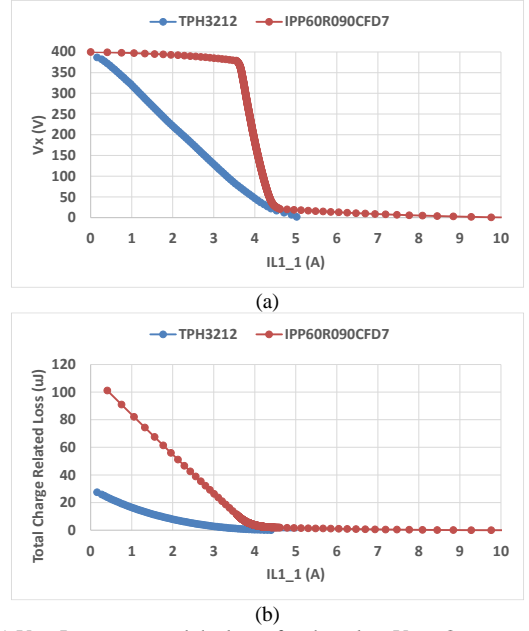

Fig. 7 (a) $V_x - I_{L1\_1}$ curve, and the loss of a phase leg, V_{dc} x $Q_{oss\_(Vdc-Vx)ToVdc}$ - $E_{oss\_(Vdc-Vx)ToVdc} + E_{oss\_VxTo0}$

III. CONVERTER EVALUATION

The GaN FET is an ideal option for the PSFB. A photo of the PSFB prototype is shown in Fig. 8. With the active snubber, the PSFB is tested across a battery voltage range from 250V to 450V and performance in difference load conditions are evaluated in this section.
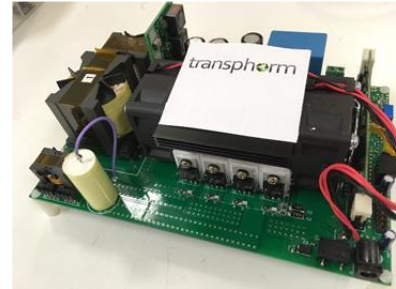

Fig. 8 TPH3212PS 200kHz 3.3kW PSFB prototype

As shown in Fig. 9 (a), efficiency of the PSFB rises with battery voltage or phase shift angle increasing, and it is above 96% over the whole battery voltage range from 250V to 450V. Notably, the arithmetic mean of efficiency is above 97% from

250V to 450V. In Fig. 9 (b), it is found that converter efficiency is still around 90% at only 10% load. Benefiting from extremely low switching loss, the GaN devices generate a minimal amount of heat and cause very low temperature rise during hard switching at 10% load, as shown in Fig. 9 (c).
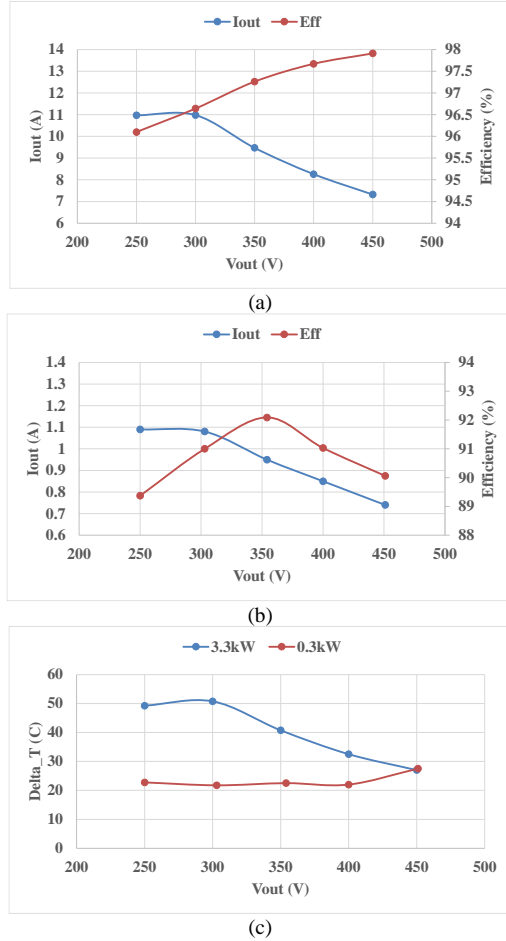

(a)

(b)

(c)

Fig. 9 Efficiency at (a) 3.3kW or 100% load and (b) 0.3kW or 10% load, and (c) device temperature rise at different load conditions.

IV. CONCLUSION AND FUTURE WORK

With GaN FETs, PSFBs become more competitive than ever. Transphorm GaN FETs offer:

- Extensive soft switching region
- Low loss during hard switching

These benefits are a result of.

- Low Output Charge (Qoss)
- Low Crossover Losses

REFERENCES

[1] https://www.belfuse.com/product/part-details?partn=TET3000-12-069RA, 2018

[2] https://www.corsair.com/ww/en/ax1600i-psu, 2018

[3] Y. F. Wu, J. Gritters, L. Shen, R. P. Smith and B. Swenson, "kV-Class GaN-on-Si HEMTs Enabling 99% Efficiency Converter at 800 V and 100 kHz," in *IEEE Transactions on Power Electronics*, vol. 29, no. 6, pp. 2634-2637, June 2014.

[4] Y.-F. Wu, Juan Guerrero, Judith McKay, K Smith, "Advances in reliability and operation space of high-voltage GaN power devices on Si substrates", *2014 IEEE Workshop on Wide Bandgap Power Devices and Applications (WiPDA), p30-32, Oct. 13, 2014.*

[5] T. Kikkawa et al., "600 V JEDEC-qualified highly reliable GaN HEMTs on Si substrates," *2014 IEEE International Electron Devices Meeting*, San Francisco, CA, 2014, pp. 2.6.1-2.6.4.

[6] G. Su, "Comparison of Si, SiC, and GaN based Isolation Converters for Onboard Charger Applications," 2018 IEEE Energy Conversion Congress and Exposition (ECCE), Portland, OR, 2018, pp. 1233-1239.

[7] H. A. Hassan, E. Iuravin, H. Cai and M. Scott, "A GaN based Dual Active Bridge Converter for Energy Storage Systems," 2018 IEEE Energy Conversion Congress and Exposition (ECCE), Portland, OR, 2018, pp. 2813-2818.

[8] F. Qi, Z. Wang and Y. Wu, "650V GaN Based 3.3kW Bi-Directional DC-DC Converter for High Efficiency Battery Charger with Wide Battery Voltage Range," 2019 IEEE Applied Power Electronics Conference and Exposition (APEC), Anaheim, CA, USA, 2019, pp. 359-364.

[9] B. Zhao, Q. Song, W. Liu and Y. Sun, "Overview of Dual-Active-Bridge Isolated Bidirectional DC–DC Converter for High-Frequency-Link Power-Conversion System," in IEEE Transactions on Power Electronics, vol. 29, no. 8, pp. 4091-4106, Aug. 2014.

[10] B. Whitaker, A. Barkley, Z. Cole, B. Passmore, T. McNutt and A. B. Lostetter, "A high-frequency, high-efficiency silicon carbide based phase-shifted full-bridge converter as a core component for a high-density on-board vehicle battery charging system," *2013 IEEE ECCE Asia Downunder*, Melbourne, VIC, 2013, pp. 1233-1239.

[11] M. Cacciato and A. Consoli, "New regenerative active snubber circuit for ZVS phase shift Full Bridge converter," *2011 Twenty-Sixth Annual IEEE Applied Power Electronics Conference and Exposition (APEC)*, Fort Worth, TX, 2011,